Traversing Scales of Brain and Behavioral Organization III: Theoretical Modeling

Viktor K. Jirsa, J.A. Scott Kelso, and Armin Fuchs

Program in Complex Systems and Brain Sciences, Center for Complex Systems, Florida Atlantic University, 777 Glades Road, Boca Raton, FL 33431, USA

1 Introduction

In coordinated movements typically several states related to different behavioral patterns can be found, e.g. different gaits of horses (Collins and Stewart 1993, Schöner et al. 1990) or different configurations among the joints for trajectory formation tasks (Buchanan et al. 1997, Kelso et al. 1991). These states have different stabilities dependent on external or internal control parameters. When such control parameters are manipulated, coordination states may become unstable and the system exhibits a transition from one state to another. These phenomena have intensively been investigated experimentally and theoretically and mathematical models have been set up reproducing the experimentally observed coordination behavior as well as predicting new effects (see (Haken 1996, Kelso 1995) for reviews). On the other hand, recent MEG and EEG experiments (Kelso et al. 1992, Wallenstein et al. 1995) have investigated the spatiotemporal brain dynamics during coordination of finger movements with external periodic stimuli. To accommodate these results, a mathematical phenomenological model was developed describing the on-going brain activity (Jirsa et al. 1994). In (Jirsa and Haken 1996a, 1996b) [Jirsa and Haken 1996a, Jirsa and Haken 1996b] a neurophysiologically motivated field theory of the spatiotemporal brain dynamics was elaborated which combined properties of neural ensembles, including their short- and long-range connections in the cortex, in addition to describing the interaction of functional units embedded into the neural sheet. This approach was applied to the brain-coordination experiment (Kelso et al. 1992) where the subject's task was to coordinate rhythmic behavior of a finger with an external acoustic stimulus. During the experiment the MEG of the subject was recorded. Complex systems, such as the brain, have the general property that they perform low-dimensional behavior during transitions from one macroscopic state to another (Cross and Hohenberg 1993, Haken 1983, 1987). This type of behavior has also been found in the analyses (Fuchs et al. 1992, Jirsa et al. 1995) of the brain data from the coordination experiment in (Kelso et al. 1992). On the basis of these analyses the phenomenological model in (Jirsa et al. 1994) describing the brain activity was derived qualitatively from the neurophysiologically motivated theory in (Jirsa and Haken 1996a, 1997).

C. Uhl (ed.), *Analysis of Neurophysiological Brain Functioning*

The goal of the present paper is to show how it may be possible to traverse levels of organization from the behavioral level to the brain level. For this purpose, we choose a bimanual coordination experiment (Kelso 1981,1984) in which a transition in coordinated behavior is observed between finger movements when a control parameter is changed. Along this example, we will treat the organization on the level of behavior (Sect. 2) and then make the the connection to the organization on the level of the brain (Sect. 3).

2 The Level of Behavior

Experimental studies by one of us (Kelso 1981,1984), as well as others (see e.g. (Carson et al. 1994) for a review) have shown that abrupt phase transitions occur in human finger movements under the influence of scalar changes in the cycling frequency. Below a critical cycling frequency two dynamical patterns or states are possible: An in-phase state where the finger movements are symmetric and an anti-phase state where the finger movements are antisymmetric. Starting the finger movements in the anti-phase state and increasing the cycling frequency, a spontaneous transition from anti-phase to in-phase is observed at a critical frequency. Beyond this frequency only the in-phase state is stable. Further, it is experimentally found that the amplitude of the finger movements decreases when the cycling frequency is increased.

In 1985 these phenomena were theoretically modeled by Haken, Kelso and Bunz (1985) by formulating a model system for the dynamics of the collective variable represented by the relative phase between the fingers. This model system was then used as a guide to establish a model for the dynamics of the component variables represented by the finger positions x_1 and x_2. These component variables perform an oscillatory behavior and interact nonlinearily. Two ordinary differential equations, again based on detailed experimental results, describe the dynamics of the individual fingers with the amplitudes x_1 and x_2. This model system reads

$$\ddot{x}_1 + (Ax_1^2 + B\dot{x}_1^2 - \gamma)\dot{x}_1 + \Omega^2 x_1 = (\dot{x}_1 - \dot{x}_2)\,(\alpha + \beta(x_1 - x_2)^2) \qquad (1)$$

$$\ddot{x}_2 + (Ax_2^2 + B\dot{x}_2^2 - \gamma)\dot{x}_2 + \Omega^2 x_2 = (\dot{x}_2 - \dot{x}_1)\,(\alpha + \beta(x_1 - x_2)^2) \qquad (2)$$

The left hand sides of (1), (2) describe the motion of the individual fingers, while the right hand sides describe the coupling.

With the goal of connecting behavioral coordination dynamics (1) and (2) to brain dynamics we introduce an alternative description of these phenomena in terms of symmetric and antisymmetric modes. These modes directly correspond to the behavioral states of the system, for which we seek correspondence at the brain level.

We define the following variables:

$$\tilde{\psi}_+ = x_1 + x_2 \qquad \tilde{\psi}_- = x_1 - x_2 \qquad (3)$$

These variables represent modes of behavior where $\tilde{\psi}_+$ corresponds to the symmetric (in-phase) mode and $\tilde{\psi}_-$ to the antisymmetric (anti-phase) mode. The back transformation onto the amplitudes of finger movement reads

$$x_1 = \frac{1}{2}(\tilde{\psi}_+ + \tilde{\psi}_-) \qquad x_2 = \frac{1}{2}(\tilde{\psi}_+ - \tilde{\psi}_-)\,. \tag{4}$$

In order to obtain the equations governing the dynamics of the new variables $\tilde{\psi}_+$, $\tilde{\psi}_-$ we subtract and sum (1), (2), respectively, and obtain

$$\begin{aligned}
&\ddot{\tilde{\psi}}_+ - \gamma\dot{\tilde{\psi}}_+ + \Omega^2\tilde{\psi}_+ + \tfrac{A}{12}\tfrac{\partial}{\partial t}(\tilde{\psi}_+^3 + 3\tilde{\psi}_-^2\tilde{\psi}_+) + \tfrac{B}{4}(\dot{\tilde{\psi}}_+^3 + 3\dot{\tilde{\psi}}_-^2\dot{\tilde{\psi}}_+) = 0\\
&\ddot{\tilde{\psi}}_- - \gamma\dot{\tilde{\psi}}_- + \Omega^2\tilde{\psi}_- + \tfrac{A}{12}\tfrac{\partial}{\partial t}(\tilde{\psi}_-^3 + 3\tilde{\psi}_+^2\tilde{\psi}_-)\\
&\qquad + \tfrac{B}{4}(\dot{\tilde{\psi}}_-^3 + 3\dot{\tilde{\psi}}_+^2\dot{\tilde{\psi}}_-) = 2\dot{\tilde{\psi}}_-\,(\alpha + \beta\tilde{\psi}_-^2).
\end{aligned} \tag{5}$$

The left hand sides of (5) represent fully symmetric (with respect to the exchange of the indices + and −), nonlinearly coupled equations. The former coupling terms with α and β in the variables x_1, x_2 now appear only in one equation solely in terms of the antisymmetric mode $\tilde{\psi}_-$.

In order to treat the system (5) analytically we make the following ansatz:

$$\tilde{\psi}_+ = R_+ e^{i\Phi_+} e^{i\Omega t} + R_+ e^{-i\Phi_+} e^{-i\Omega t} \tag{6}$$

$$\tilde{\psi}_- = R_- e^{i\Phi_-} e^{i\Omega t} + R_- e^{-i\Phi_-} e^{-i\Omega t} \tag{7}$$

where R_+, R_- denote real time dependent amplitudes and Φ_+, Φ_- the corresponding time dependent phases. Inserting this ansatz into (5) and performing two approximations well known in nonlinear oscillator theory (rotating wave approximation, slowly varying amplitude approximation, see e.g. (Haken (1983))) we obtain the following equations for the amplitudes

$$\begin{aligned}
\dot{R}_+ &= \tfrac{1}{2}\gamma R_+ - a(\Omega)\,(R_+^2 + 2R_-^2 + R_-^2\cos 2(\Phi_- - \Phi_+))\,R_+\\
\dot{R}_- &= \tfrac{1}{2}\gamma R_- - a(\Omega)\,(R_-^2 + 2R_+^2 + R_+^2\cos 2(\Phi_+ - \Phi_-))\,R_- + \alpha R_- + \beta R_-^3
\end{aligned} \tag{8}$$

and for the phases

$$\dot{\Phi}_+ = -a(\Omega)R_-^2 \sin 2(\Phi_- - \Phi_+) \tag{9}$$

$$\dot{\Phi}_- = -a(\Omega)R_+^2 \sin 2(\Phi_+ - \Phi_-) \tag{10}$$

where $a(\Omega) = 1/8(A + 3B\Omega^2)$. Defining the new variable $\phi = \Phi_+ - \Phi_-$ we can rewrite (9), (10) as

$$\dot{\phi} = -a(\Omega)(R_+^2 + R_-^2)\sin 2\phi \tag{11}$$

which has the only stable solutions $\phi = \frac{\pi}{2}, \frac{3\pi}{2}$ for nontrivial amplitudes R_+, R_-. Thus (8) can be reduced to

$$\begin{aligned} \dot{R}_+ &= \tfrac{1}{2}\gamma R_+ - a(\Omega)\,(R_+^2 + R_-^2)\,R_+ &&= -\frac{\partial V}{\partial R_+} \\ \dot{R}_- &= \tfrac{1}{2}\gamma R_- - a(\Omega)\,(R_+^2 + R_-^2)\,R_- + \alpha R_- + \beta R_-^3 &&= -\frac{\partial V}{\partial R_-} \end{aligned} \tag{12}$$

where the dynamics of R_+, R_- can be expressed in terms of a gradient dynamics with the potential

$$V = -\frac{1}{4}\gamma(R_+^2 + R_-^2) + \frac{1}{4}a(\Omega)\,(R_+^2 + R_-^2)^2 - \frac{1}{2}\alpha R_-^2 - \frac{1}{4}\beta R_-^4 \tag{13}$$

A linear stability analysis of (12) yields the same results as in (Haken et al. 1985) and can be graphically presented in terms of the potential V in (13). In Fig. 1 (upper row) the potential V is plotted in dependence of R_+ and R_- as the control parameter Ω increases from left to right. Here the R_--axis points out of the page. The corresponding isoclines of V are plotted below in arbitrary units of R_+, R_-. Below the critical frequency bistability is present (left two pictures), i.e. either the symmetric or the antisymmetric mode is present. At the critical frequency Ω_c (third picture) the antisymmetric mode becomes unstable and only the symmetric mode remains for higher frequencies (right picture).

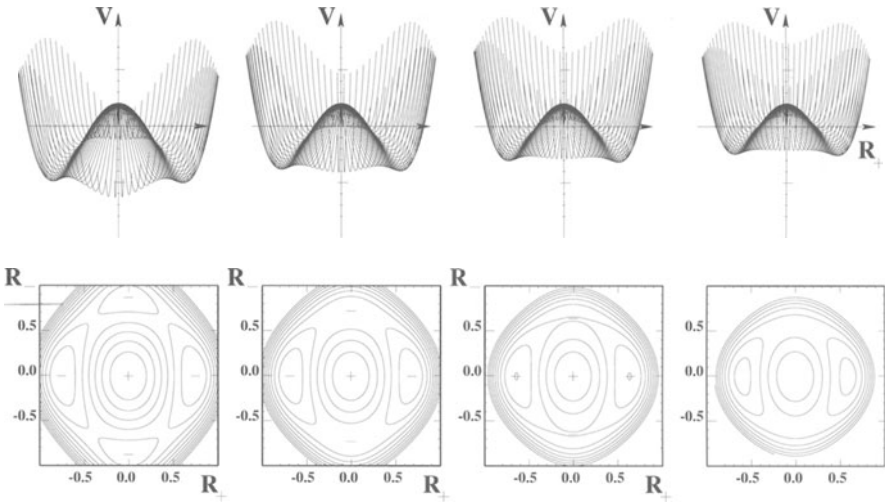

Fig. 1. The potential V is plotted (top row) in dependence of R_+ and R_- as the frequency increases from left to right. The axis of R_- points out of the page. The scale on the axes is in arbitrary units. The isoclines of the potential V are plotted in dependence of the oscillator amplitudes R_+, R_-. The plus sign marks a local maximum, the minus sign a local minimum

3 The Level of Brain

In the framework of this paper we will use the behavioral mode system (5) as a guideline to traverse scales of organization from the behavioral level to the brain level. First we briefly review a field theoretical description of neural activity recently developed by Jirsa & Haken (1996a, 1996b, 1997), then we specify the neural field equation with respect to the bimanual coordination experiment and discuss it in detail.

3.1 Field Theoretical Description of Neural Activity

Let us consider a $(n-1)$-dimensional closed surface Γ representing the neocortex in a n-dimensional space. This medium Γ shall consist of neural ensembles to which we assign two state variables describing their activity: Dendritic currents generated by active synapses cause *waves* of extracellular fields which can be measured by the EEG (Freeman 1992) and intracellular fields measurable by the MEG (Williamson and Kaufman 1987). Action potentials generated at the somas of neurons correspond to *pulses*. We call the magnitude of the neural ensemble average of the waves the wave activity $\psi_j(x,t)$ with $j = \mathrm{e}, \mathrm{i}$ where the indices distinguish excitatory and inhibitory activity and the magnitude of the neural ensemble average of the pulses the pulse activity $\psi_j(x,t)$ with $j = \mathrm{E}, \mathrm{I}$ distinguishing excitatory and inhibitory pulses. The location in Γ is denoted by x, the time point by t. These scalar quantities are related to each other via conversion operations (Freeman 1992) which we define as

$$\psi_j(x,t) = \int_\Gamma \mathrm{d}X \; f_j(x,X) H_j(x,X,t) \; , \tag{14}$$

where $j = \mathrm{e}, \mathrm{i}, \mathrm{E}, \mathrm{I}$. Here the function $H_j(x,X,t)$ represents the output of a conversion operation and $f_j(x,X)$ the corresponding distribution function depending on the spatial connectivity. From experimental results of Freeman (1992) it is known that the conversion from wave to pulse is sigmoidal within a neural ensemble, however the conversion from pulse to wave is also sigmoidal, but constrained to a linear small-signal range. Assuming that excitatory neurons only have excitatory synapses, inhibitory neurons only inhibitory synapses (which is generally true (Abeles 1991)) we obtain the following relations between conversion output and pulses

$$H_\mathrm{e}(x,X,t) = S\left[\psi_\mathrm{E}\left(X, t - \frac{\mid x-X \mid}{v}\right)\right] \approx a_\mathrm{e}\psi_\mathrm{E}\left(X, t - \frac{\mid x-X \mid}{v}\right) \tag{15}$$

$$H_\mathrm{i}(x,X,t) = S\left[\psi_\mathrm{I}\left(X, t - \frac{\mid x-X \mid}{v}\right)\right] \approx a_\mathrm{i}\psi_\mathrm{I}\left(X, t - \frac{\mid x-X \mid}{v}\right) \tag{16}$$

and between conversion output and waves

$$H_{\mathrm{E}}(x,X,t) = S_{\mathrm{e}}\left[\psi_{\mathrm{e}}\left(X, t - \frac{\mid x - X \mid}{v}\right) - \psi_{\mathrm{i}}\left(X, t - \frac{\mid x - X \mid}{v}\right) + p_{\mathrm{e}}\left(X, t - \frac{\mid x - X \mid}{v}\right)\right], \tag{17}$$

$$H_{\mathrm{I}}(x,X,t) = S_{\mathrm{i}}\left[\psi_{\mathrm{e}}\left(X, t - \frac{\mid x - X \mid}{v}\right) - \psi_{\mathrm{i}}\left(X, t - \frac{\mid x - X \mid}{v}\right) + p_{\mathrm{i}}\left(X, t - \frac{\mid x - X \mid}{v}\right)\right] \tag{18}$$

External input $p_j(x,t)$ is realized such that afferent fibers make synaptic connections and thus $p_j(x,t)$ appears only in (17), (18). Here a_e, a_i are constant parameters denoting synaptic weights, v the propagation velocity and S, S_j the sigmoid functions of a class j ensemble.

Let us now make the following considerations: We are interested in a spatial scale of several cm and temporal scale of 100 msec which is relevant in EEG and MEG. Intracortical fibers (excitatory and inhibitory) typically have a length of 0.1 cm, corticocortical (only excitatory) fiberlengths range from about 1 cm to 20 cm (Nunez 1995). Cortical propagation velocities have a wide range from 0.2 m/sec (Miller 1987) up to 6–9 m/sec (Nunez 1995). With an average velocity of 1 m/sec this yields propagation delays of 1 msec for the intracortical fibers and 10 msec to 200 msec for the corticocortical fibers. Synaptic delays and refractory times are of the order 1 msec, the neuronal membrane constant is in the range of several msec (Braitenberg and Schüz 1991). From this brief summary we see that the spatial and temporal scales vary considerably. The distribution of the intracortical fibers is very homogeneous (Braitenberg and Schüz 1991), but the distribution of the corticocortical fibers is not (estimates are that 40% of all possible corticortical connections are realized for the visual areas in the primate cerebral cortex (Felleman and Van Essen 1991)). We assume the corticocortical fiber distributions to be homogeneous as a first approximation. Using the discussed temporal and spatial hierarchies the dynamics of the system (14)–(18) can be systematically reduced (see (Jirsa and Haken 1996a,1996b,1997) for details): the fast dynamics ($<<$ 100 msec) becomes either instantaneous or can be eliminated and the spatial scales smaller than 1cm become point-like. Then the entire dynamics of the system can be described in terms of the slowest variable $\psi_{\mathrm{e}}(x,t)$ and a modified external input now denoted by $p(x,t)$. The dynamics of $\psi_{\mathrm{e}}(x,t)$ is given by

$$\psi_{\mathrm{e}}(x,t) = a_{\mathrm{e}} \int_{\Gamma} \mathrm{d}X \, f_{\mathrm{e}}(x - X) \times S_{\mathrm{e}}\left[\rho\,\psi_{\mathrm{e}}\left(X, t - \frac{\mid x - X \mid}{v}\right) + p\left(X, t - \frac{\mid x - X \mid}{v}\right)\right], \tag{19}$$

where ρ is a density of excitatory fibers, modified due to the elimination of the other variables. Note that from the equations (14)-(18) the models by Wilson & Cowan (1972,1973) in terms of pulse activities and by Nunez (1974,1995) in terms of wave activities can be derived and are connected by our approach.

Until now the dimension of the cortical surface has been kept general. Here we want to specify $n = 2$, meaning that Γ represents a closed 1-dimensional loop. Such a geometry has been reported by Nunez (Nunez 1995) to be a good approximation when macroscopic EEG dynamics is considered under more qualitative aspects of dynamics like changes of dispersion relations. In the following sections we will perform a low-dimensional mode decomposition in which case the chosen geometry suffices for a discussion of the temporal mode dynamics. Using the method of Green's functions (Jirsa and Haken 1997) the above integral equation (19) can be rewritten as a nonlinear partial differential equation

$$\ddot{\psi} + (\omega_0^2 - v^2 \triangle)\, \psi + 2\omega_0 \dot{\psi} = a_e \left(\omega_0^2 + \omega_0 \frac{\partial}{\partial t}\right) S[\rho\, \psi(x,t) + p(x,t)] \quad (20)$$

where $\omega_0 = v/\sigma$ and we dropped the indices e. Here we call $\psi(x,t)$ the neural field. The interaction of functional units with the cortical sheet Γ is represented by the external input signals $p_j(x,t)$, where $p(x,t) = \sum_j p_j(x,t)$ and the output signals $\bar{\psi}_j(t)$. A functional unit can include subcortical structures such as the projections of the cerebellum on the cortex or specific functional areas like the motor cortex. Anatomically these areas are obviously defined via their afferent and efferent fibers connecting to the cortical sheet. In the context of the present theory dealing with dynamics on a larger spatiotemporal scale, i.e. wavelengths in the regime of several cm, it is more appropriate to identify the spatial localizations of the functional input units with the spatial structures which are generated by the time dependent input signals $z_j(t)$, open to observation in the EEG/MEG. In the case of a finger movement this spatial structure $\beta_j(x)$ corresponds to the well-known dipolar mode in the EEG/MEG located over the contralateral motor areas. Thus such a functional input unit is defined as

$$p_j(t) = \beta_j(x)\, z_j(t)\ . \quad (21)$$

Similarly, an output signal $\bar{\psi}_j(t)$ sent to non-cortical areas is picked up from the cortical sheet according to

$$\bar{\psi}_j(t) = \int_\Gamma \mathrm{d}x\, \beta_j(x) \psi(x,t)\ , \quad (22)$$

where $\beta_j(x)$ defines the spatial localization of the jth functional output unit.

In summary, the field theoretical approach presented here aims at a description of the spatiotemporal brain dynamics on the scale of several cm and 100 msec. These scales emphasize the corticocortical connections and allow

the derivation of (19) in one field variable $\psi(x,t)$ governing the spatiotemporal dynamics. Focussing on the dynamical aspects of the interaction of only a few modes in the following sections, a cortical representation of a closed strip is chosen.

3.2 Neural Field Theory of Bimanual Coordination

The neural areas subserving bimanual coordination are numerous and diverse. The cortex, through intracortical connections and long loop, reciprocal pathways to the basal ganglia and cerebellum, obviously plays a crucial role. Propriospinal and brainstem networks are also involved. Wiesendanger et al. (Wiesendanger et al. 1994) in a recent review of lesion studies in humans and non-human primates implicate lateral premotor cortex, supplementary motor area, parietal association cortex and the anterior corpus callosum (among others) in goal-directed bimanual coordination. Though many kinds of cortical lesions can affect bimanual movements, objective measures of spatiotemporal organization are rare in studies of patient populations. In the context of the present work, Tuller & Kelso (1989) showed that in-phase and anti-phase movements of the fingers were preserved in split-brain patients. Other phase relations were much more difficult for split brains to produce compared to normal subjects. Anatomical and physiological evidence for bilateral control of each cortical area may explain why callosal damage and unilateral cortical lesions tend to produce only transient disturbances of bimanual coordination (Wiesendanger et al. 1994).

For present purposes, we consider a simplified scheme in which cortical areas interact in a cooperative fashion to produce goal-directed bimanual coordination (see Fig. 2). Evidence for bilateral activation of primary motor cortices during a bimanual task in which both index fingers are simultaneously moved (see e.g. (Kristeva et al. 1991)), is consistent with our double representation of "motor areas" in Fig. 2. Likewise, the presence of movement evoked fields in both postcentral cortices corresponding to reafferent activity from the periphery during bimanual movements (Kristeva et al. 1991) justifies the two "sensorimotor areas" in our model. Thus, motor signals are conveyed from the motor areas in the cortical sheet to the individual fingers, sensorimotor signals carrying information about the finger movements are conveyed to the sensorimotor areas of the brain. Please note that we assign the same index l (r) to the left (right) finger and its contralateral hemisphere in order to keep the notation in the following mathematical treatment as simple as possible. Here we deal with the following situation as shown in Fig. 2: two input units localized at $\beta_{ls}(x)$ (left hemisphere, sensorimotor), $\beta_{rs}(x)$ (right hemisphere, sensorimotor) and two output units localized at $\beta_{lm}(x)$ (left hemisphere, motor), $\beta_{rm}(x)$ (right hemisphere, motor) are embedded into a one-dimensional closed neural strip. The origin of the underlying coordinate system is located between the two hemispheres where L is the length of the neural strip. Anatomical considerations imply as a first approximation

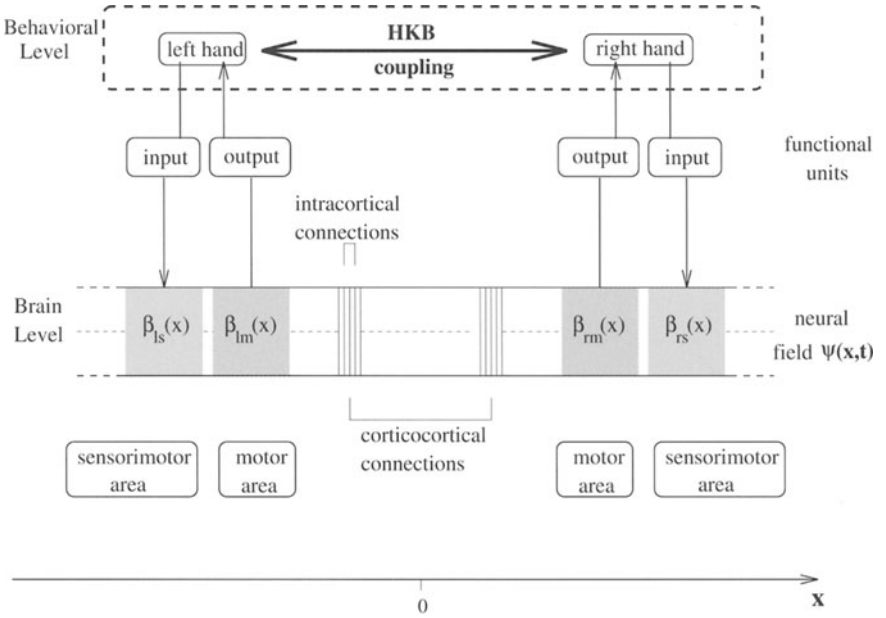

Fig. 2. Two input units localized at $\beta_{ls}(x)$ (sensorimotor, left hemisphere), $\beta_{rs}(x)$ (sensorimotor, right hemisphere) and two output units localized at $\beta_{lm}(x)$ (motor, left hemisphere), $\beta_{rm}(x)$ (motor, right hemisphere) are embedded into a one-dimensional closed neural strip whose activity is described by the field $\psi(x,t)$

the following symmetries:

$$\begin{aligned} \beta_{ls}(x) &= \beta_{rs}(-x) \\ \beta_{lm}(x) &= \beta_{rm}(-x) \end{aligned} \tag{23}$$

The output signal, here the motor field, is defined according to (22) and is conveyed to the corresponding finger where $z_l(t) = x_1(t)$, $z_r(t) = x_2(t)$ denote the extensions of the left and right finger movements, respectively. The motor movement $z_j(t)$ with $j = l, r$ shall be described phenomenologically as a function f of the motor field $\bar{\psi}_j(t)$ and, in order to take phase shifts into account, its derivative $\dot{\bar{\psi}}_j(t)$:

$$z_j(t) = f(\bar{\psi}_j(t), \dot{\bar{\psi}}_j(t)) \approx f_0 + f_1\, \bar{\psi}_j(t) + f_2\, \dot{\bar{\psi}}_j(t) + \ldots \tag{24}$$

where $f(\bar{\psi}_j(t), \dot{\bar{\psi}}_j(t))$ denotes a nonlinear function which we expanded into a Taylor function in terms of $\bar{\psi}_j(t)$ and $\dot{\bar{\psi}}_j(t)$ and truncated after the linear terms as an approximation. The constant f_0 describes a constant amplitude shift and can be set to zero for a rhythmic movement. See also (Jirsa and Haken 1997) for a treatment of the sensorimotor feedback loop in terms of driven oscillators. In the following discussion we will consider the limit case

$f_1 \neq 0, f_2 = 0$. A discussion of the other limit $f_1 = 0, f_2 \neq 0$ gives analogeous results. With (22),(24) and $f_1 \neq 0, f_2 = 0$ the sensorimotor feedback is now given by

$$p_j(x,t) = \beta_{js}(x) z_j(t) = c_0 \, \beta_{js}(x) \int_{-L/2}^{L/2} \beta_{jm}(x) \psi(x,t) \, \mathrm{d}x \tag{25}$$

and the feedback loops of the motor and sensorimotor units are closed.

We are now in a position to specify the field equation (20) as follows

$$\ddot{\psi} + (\omega_0^2 - v^2 \triangle)\psi + 2\omega_0 \dot{\psi} = a_e \left(\omega_0^2 + \omega_0 \frac{\partial}{\partial t} \right) S[\rho\psi + p_l(x,t) + p_r(x,t)] \, . \tag{26}$$

The field $\psi(x,t)$ can also always be written in terms of symmetric and antisymmetric contributions

$$\psi(x,t) = \underbrace{\frac{1}{2}(\psi(x,t) + \psi(-x,t))}_{\psi^+(x,t)} + \underbrace{\frac{1}{2}(\psi(x,t) - \psi(-x,t))}_{\psi^-(x,t)} \, . \tag{27}$$

Next, we make an assumption about the spatial pattern underlying the temporal dynamics of $\psi^+(x,t)$ and $\psi^-(x,t)$. In the bimanual coordination experiment a transition from one pattern to another is observed on the behavioral level. In this case the theory of dynamical systems, in particular synergetics (Haken (1983),1987), predicts low dimensional behavior of the system under consideration and we expect to observe low-dimensional transition phenomena on the brain level, too. Further, in previous analyses of brain-behavior experiments (Fuchs et al. 1992, Jirsa et al. 1995) involving behavioral transitions during coordination with external stimuli low-dimensional spatiotemporal brain dynamics was found and could be described in terms of two spatial modes. Here we deal with the different situation of the coordination of two limbs. But since a similar phase transition in behavior has also been observed, we assume to a first approximation that each contribution $\psi^+(x,t)$ and $\psi^-(x,t)$ is dominated by one spatial pattern and factorizes

$$\begin{aligned} \psi^+(x,t) &\approx g_+(x) \, \psi_+(t) \\ \psi^-(x,t) &\approx g_-(x) \, \psi_-(t) \end{aligned} \tag{28}$$

if only standing waves are present. The assumption of two dominating spatial modes is crucial for the following mathematical analysis and experimentally easy to test. If this assumption is confirmed, higher order structures of the dynamics can be included following the lines of (Jirsa et al. 1995) in which the reproduction of the experimental spatiotemporal signal could be improved by adding more spatial modes whose temporal dynamics depends only on the dynamics of the prior modes. The ansatz (28) can also be expanded for higher dimensions or traveling waves, but first, this will increase the complexity of the analytical treatment considerably and second, in most cases it will not

lead to the same results as in the case of two dominating spatial modes. For these reasons the hypothesis (28) is the first to be tested experimentally.

A complex system whose dynamics is governed by a nonlinear evolution law may perform phase transitions from one stationary state to another when a control parameter is varied. Close to the transition point the dynamics of this system is governed by the first leading orders of the nonlinearities (Haken (1983),1987). Here we express the sigmoid function $S[n]$ by the logistic function

$$S[n] = \frac{1}{1+\exp(-4an)} - \frac{1}{1+\exp(4a)}\,, \tag{29}$$

where a denotes the sensitivity coefficient of response of the corresponding neural population. We expand (29) into a Taylor series around $n = 0$ up to third order in n and obtain

$$S[n] \approx an - \frac{4}{3}a^3 n^3 \tag{30}$$

which is a good approximation for values an smaller than 1. Projecting the neural field equation (26) onto $g_+(x)$ and $g_-(x)$ following the lines in (Jirsa and Haken 1996a,1997), we obtain

$$\ddot{\psi}_+ + 2\omega_0\dot{\psi}_+ + \Omega_+^2\psi_+ = a_e\left(\omega_0^2 + \omega_0\frac{\partial}{\partial t}\right)\left[af_{10}\psi_+ - \frac{4}{3}a^3(f_{30}\psi_+^3 + 3f_{12}\psi_-^2\psi_+\right] \tag{31}$$

$$\ddot{\psi}_- + 2\omega_0\dot{\psi}_- + \Omega_-^2\psi_- = a_e\left(\omega_0^2 + \omega_0\frac{\partial}{\partial t}\right)\left[af_{01}\psi_- - \frac{4}{3}a^3(f_{03}\psi_-^3 + 3f_{21}\psi_+^2\psi_-\right] \tag{32}$$

where

$$\Omega_i^2 = \omega_0^2 - v^2\int_{-L/2}^{L/2}\triangle g_i(x)\,\mathrm{d}x \qquad \text{with} \qquad i = +,- \tag{33}$$

and the terms f_{ij} with $i,j = 1,2,3$ are constant parameters which are given in the appendix.

So far we tackled the level of the brain, let us now traverse the scales of organization by referring back to the behavioral level where the equations governing the behavioral dynamics are known from (5). Here we take these equations as a guide to obtain conditions which restrict the solution space of (31), (32).

In (3) we expressed the behavioral modes in terms of finger displacements. With (24) we can express the behavioral modes in terms of the neural field

$$\tilde{\psi}_+(t) = z_l(t) + z_r(t) = c_0\int_{L/2}^{L/2}(\beta_{lm}(x) + \beta_{rm}(x))\,\psi(x,t)\,\mathrm{d}x \tag{34}$$

$$\tilde{\psi}_-(t) = z_l(t) - z_r(t) = c_0\int_{L/2}^{L/2}(\beta_{lm}(x) - \beta_{rm}(x))\,\psi(x,t)\,\mathrm{d}x \tag{35}$$

If we take our hypothesis (28) of two dominating spatial modes into account, the behavioral modes can be expressed as

$$\tilde{\psi}_+(t) = c_0\,\psi_+(t)\int_{L/2}^{L/2}(\beta_{lm}(x)+\beta_{rm}(x))\,g_+(x)\,\mathrm{d}x = c_+\psi_+(t) \tag{36}$$

$$\tilde{\psi}_-(t) = c_0\,\psi_-(t)\int_{L/2}^{L/2}(\beta_{lm}(x)-\beta_{rm}(x))\,g_-(x)\,\mathrm{d}x = c_-\psi_-(t) \tag{37}$$

where c_+, c_- are constant. In the present framework, it turns out that in the bimanual coordination case the symmetric (antisymmetric) behavioral mode is proportional to the symmetric (antisymmetric) brain mode. As a consequence the dynamical system (5) of the behavioral modes and the system (31), (32) of the brain modes should be equivalent. This requires $\omega_0^2 \ll \omega_0\partial/\partial t$ which implies on the considered time scales (see also (Jirsa and Haken 1997) where this limit was used) that the mean corticocortical fiber length is large. We rewrite (31), (32) as

$$\begin{aligned}
&\ddot{\psi}_+ - \gamma\dot{\psi}_+ + \Omega_+^2\psi_+ + b\tfrac{\partial}{\partial t}(f_{30}\psi_+^3 + 3f_{12}\psi_-^2\psi_+) = 0\\
&\ddot{\psi}_- - \gamma\dot{\psi}_- + \Omega_-^2\psi_- + b\tfrac{\partial}{\partial t}(f_{30}\psi_-^3 + 3f_{21}\psi_+^2\psi_-) = 2\dot{\psi}_-\,(\alpha+\beta\psi_-^2)
\end{aligned} \tag{38}$$

where

$$\begin{aligned}
b &= 4/3a_e a^3\omega_0 & \gamma &= a_e a\omega_0 f_{10} - 2\omega_0\\
\alpha &= 1/2a_e a\omega_0(f_{01}-f_{10}) & \beta &= -2a_e a^3\omega_0(f_{03}-f_{30})
\end{aligned} \tag{39}$$

The system (38) is structurally equivalent to the dynamical system (5) for the behavioral modes. Note that in the latter system the Rayleigh terms with the parameter B were introduced in order to obtain a frequency dependence of the oscillator amplitude (see (Haken et al. 1985)). An alternative way to achieve this dependence is to introduce frequency dependent parameters in (5), e.g. $A(\Omega) = A + 3B\Omega^2$ or $\gamma = \gamma(\Omega)$ which yields the same results as a Rayleigh term. If $f_{12} = f_{21}$ and $\Omega_+ = \Omega_-$, then the lhs of (38) represents a fully symmetric system with respect to the coupling terms. The rhs of the second equation in (38) is a consequence of the difference between the spatial overlap of *functional units – symmetric brain mode* and *functional units – antisymmetric brain mode.* From the behavioral mode system (5) we know the necessary condition $\alpha < 0, \beta > 0$ which leads to the nontrivial restriction $f_{01} < f_{10}$, $f_{03} < f_{30}$ and implies a greater spatial overlap of the considered functional units with the symmetric brain mode.

3.3 Numerical Treatment

In order to illustrate our more general results of the previous section we choose a simple example for a specific set of brain modes and localized functional units. The motor and sensorimotor areas on the right hemisphere are localized as follows

$$\beta_{rm}(x) = \beta_{rs}(x) = \begin{cases} \frac{2\pi}{L} & -\epsilon \leq x \leq \frac{L}{4} \\ 0 & \text{otherwise} \end{cases} \tag{40}$$

and on the left hemisphere

$$\beta_{lm}(x) = \beta_{ls}(x) = \begin{cases} \frac{2\pi}{L} & -\frac{L}{4} \leq x \leq \epsilon \\ 0 & \text{otherwise} \end{cases} \tag{41}$$

and satisfy the required anatomical symmetry (23). For reasons of simplicity we choose the motor and sensorimotor units on the same hemisphere to be identical in the numerical treatment. The sensorimotor feedback is specified for the limit, $f_1 \neq 0, f_2 = 0$, according to (24). We introduce a frequency dependent function $\gamma_0(\Omega)$ into the linear damping $G_0(\Omega) = 2\omega_0 + \gamma_0(\Omega)$ on the lhs of (26) which causes a frequency dependence of the wave amplitude and thus a frequency dependence of the finger movements as experimentally observed. For $\gamma_0(\Omega) = 0$ the original field equation is present. In our specific example (40)–(41) the mean field $\bar{\psi}(x,t)$, equivalent to the homogeneous mode, has to remain constant. To ensure this, we introduce a linear mean field damping $\dot{\bar{\psi}}(x,t)$ into (26). Using a semi-implicit Forward-Time-Central-Space procedure we integrate the field equation (26) numerically. The functional units are localized according to (40), (41) and the edges of the localization functions were smoothed for reasons of numerical stability. Periodic boundaries were chosen. The parameters used in the numerical simulations are: $\omega_0 = 2\pi\, 0.1$, $v = 0.152$, $a_e = 1$, $a = 0.4$, $\rho = 0.5$, $c_0 = 2$, extension of the neural strip $L = 1$, spatial overlap of the localization functions $\epsilon = 0.025$. Here the space unit corresponds to 1 m and the time unit to 100 msec. This parameter range is realistic: the corticocortical propagation velocity v is in the 1 m/sec range, the extension of the neural sheet L is in the 1 m range and the long range connectivity $\sigma = v/\omega_0$ is in the 10 cm range.

In the bottom left corner of Fig. 3 the localization of the functions $\beta_{li}(x)$, $\beta_{ri}(x)$ with $i = m, s$ is shown within the neural strip, above that the symmetric mode $g_+(x)$ and the antisymmetric mode $g_-(x)$ are shown. The color code used is given in the second row on the lhs. On the rhs of Fig. 3 four rows each consisting of a space-time plot and time series are given. In each space-time plot the color-coded field $\psi(x,t)$ is plotted where the spatial domain x is vertical and the temporal domain t horizontal as indicated by the arrows in the top left corner. In the graphs under the space-time plots the field $\psi(x,t)$ is projected onto the symmetric mode $g_+(x)$ (blue line) and the antisymmetric mode $g_-(x)$ (red line) plotted over time t (in sec). The first two rows describe the situation before the pretransition with $\gamma_0(\Omega) = 0$. Two possible states are shown: In the top row the antisymmetric mode $g_-(x)$ dominates; in the second row, it is the symmetric mode $g_+(x)$ that dominates. Increasing the damping to $\gamma_0(\Omega) = 0.3$, the antisymmetric mode becomes unstable and performs a transition to the symmetric state. This transition is shown in the third row. The symmetric mode remains stable in the posttransition regime as can be seen in the bottom row. Hence in the case $\epsilon > 0$, bistability is

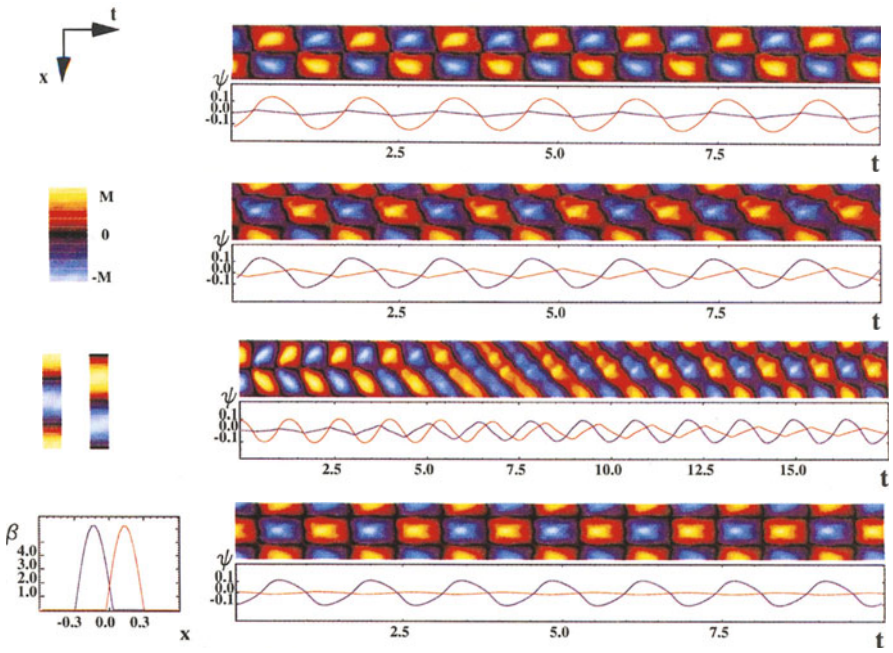

Fig. 3. The overlap of the localization functions $\beta_{ij}(x)$ is shown in the bottom left corner. The activity of the field $\psi(x,t)$ is plotted over the time t (horizontal) and the space x (vertical), together with the time series of the symmetric mode $g_+(x)$ (blue line) and the antisymmetric mode $g_-(x)$ (red line). The top two rows correspond to the pretransition region $\gamma_0(\Omega) = 0$, the bottom two rows to the posttransition region $\gamma_0(\Omega) = 0.3$

present in the pretransition regime and monostability in the posttransition regime. For $\epsilon = 0$ no transition is observed and bistability is preserved for the entire control parameter regime.

3.4 Preliminary Experimental Test of Theoretical Predictions

A brain-behavior-experiment has been performed by Kelso et al. (1994) in which subjects moved their left and right index fingers in time with an auditory metronome presented to both ears in ascending frequency plateaus of ten cycles each. The initial metronome frequency was 2.0 Hz and increased by 0.2 Hz for each plateau with a total number of eight plateaus. The subject was instructed to move the right finger anti-phase and the left finger in-phase with the metronome, and switched spontaneously to a movement pattern with both fingers in-phase as the metronome frequency increased to the fourth plateau (2.6 Hz). During the experiment magnetic field measurements of brain activity were obtained with a whole-head, 64-channel SQuID magnetometer at a sampling frequency of 250 Hz with a 40 Hz low-pass filter.

Each subject performed 5 blocks of 10 runs each. In the following we want to check these experimental data against the theoretical predictions above. Note that the experimental set-up (auditory metronome) and the subject's instructions differ somewhat from the experimental conditions of the present paper. Thus the following experimental results have to be considered a preliminary test of the presented theory.

In order to test our theoretical predictions of the previous sections we perform a Karhunen–Loève Decomposition (KL) (see e.g. Fuchs et al. (1992) and this volume) of the MEG data on each frequency plateau separately. A KL decomposition decomposes a spatiotemporal signal $\psi(x,t)$ into orthogonal spatial modes and corresponding time-dependent amplitudes such that a least-square error E is minimized and the KL modes have maximum variance. The normalized KL eigenvalue $\lambda = 1 - E$ is a measure for the contribution of a KL mode to the entire spatiotemporal signal. Figure 4 shows the first KL mode (top row) plotted over the movement frequency. The orientation of the modes is such that the nose is on the top indicated by the triangle and their color coding (after normalization) is given on the bottom. Before the transition at 2.6 Hz we observe a constant spatial pattern, after the behavioral transition (2.8–3.2 Hz) a different structure (increased activity on the right hand side of the mode contributing to a more antisymmetric shape) is observed in the first KL mode which is similar over the posttransition plateaus.

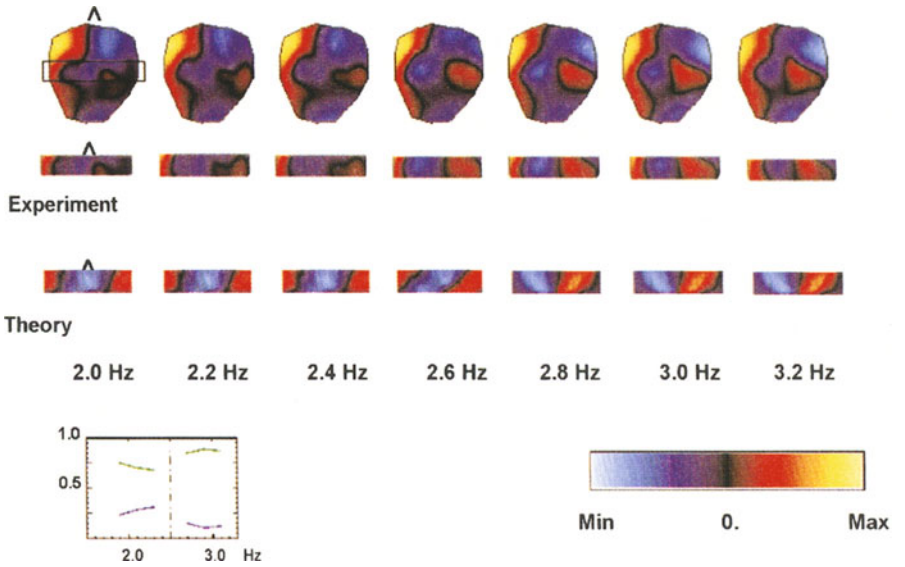

Fig. 4. Top and middle row: MEG map of first KL mode with extracted neural strip containing primary motor and sensorimotor areas plotted over movement frequency. Bottom row: Numerically simulated patterns. Bottom left: Quantification of symmetry of first KL mode (green: antisymmetric, blue: symmetric)

We extract a strip of activity from the spatial MEG patterns which is located mainly over the primary motor and sensorimotor areas (Fig. 4 middle row) and compare it with the activity of the numerically simulated data (bottom row). Note that in the numerical simulations the terms symmetric/antisymmetric apply to current distributions and hence to patterns to be observed in the EEG. Current flowing in apical dendrites of pyramidal cells generates a magnetic field in a plane orthogonal to the currents. Thus, spatial antisymmetric (symmetric) patterns in the MEG correspond to symmetric (antisymmetric) current distributions, and we reversed the symmetry of the numerically simulated patterns in Fig. 4 for better comparison.

The degree of symmetry s of the experimental first KL mode is quantified and plotted over the frequency in the bottom left corner. The transition plateau is indicated by the vertical dotted line. In the pretransition region the first KL mode is about 70% antisymmetric (green line) and 30% symmetric (blue line), whereas after the transition the antisymmetric contribution increases to 90% and the symmetric contribution decreases to 10%.

In the temporal domain (not shown in Fig. 4) almost the entire power of the first KL mode is in the Fourier component of the movement frequency for all plateaus. There is no transition in the relative phase between the amplitude of the first KL mode and the metronome which always remains in-phase with the non-switching finger movement as required by our theoretical predictions.

4 Summary

The main point of the present paper is to show how it is possible to derive the phenomenological nonlinear laws at the behavioral level from models describing brain activity. For the paradigmatic case of bimanual coordination we briefly reviewed the collective and component level of description of the behavioral dynamics. We proceeded by transforming the behavioral model on the component level onto a model describing the dynamics of the behavioral modes. The behavioral level was connected to the brain level by deriving the behavioral model on the mode level from a recently developed field theoretical description of brain activity. For the derivation the crucial points were the assumption of bimodal brain dynamics and the interplay between functional input and output units in the neural sheet. Here the comparison of behavioral and brain level serves as a guide to consistency of both descriptions. We made theoretical predictions about the global brain dynamics and presented a preliminary experimental test which gives strong indications that the predicted spatiotemporal dynamics is present during bimanual coordination tasks.

Acknowledgements

This research was supported by NIMH (Neursciences Research Branch) Grant MH42900, KO5 MH01386 and the Human Frontiers Science Program. Fur-

ther, we wish to thank Hermann Haken for many interesting discussions. VKJ gratefully acknowledges a fellowship from the *Deutsche Forschungsgemeinschaft.*

A Explicit Forms of Coupling Integrals

We define

$$f_+(x) = \rho g_+(x) + c_0 \left(\beta_{ls}(x) + \beta_{rs}(x)\right) \int_{-L/2}^{L/2} \beta_{lm}(x) g_+(x)\, \mathrm{d}x \tag{42}$$

$$f_-(x) = \rho g_-(x) + c_0 \left(\beta_{ls}(x) - \beta_{rs}(x)\right) \int_{-L/2}^{L/2} \beta_{lm}(x) g_-(x)\, \mathrm{d}x \tag{43}$$

and give the explicit forms of the coupling integrals f_{ij} in (31),(32) as

$$f_{10} = \int_{-L/2}^{L/2} g_+(x)\, f_+(x)\, \mathrm{d}x \qquad f_{01} = \int_{-L/2}^{L/2} g_-(x)\, f_-(x)\, \mathrm{d}x \tag{44}$$

$$f_{30} = \int_{-L/2}^{L/2} g_+(x)\, f_+(x)^3\, \mathrm{d}x \qquad f_{03} = \int_{-L/2}^{L/2} g_-(x)\, f_-(x)^3\, \mathrm{d}x \tag{45}$$

$$f_{12} = \int_{-L/2}^{L/2} g_+(x) f_+(x) f_-(x)^2 \mathrm{d}x \quad f_{21} = \int_{-L/2}^{L/2} g_-(x) f_+(x)^2 f_-(x) \mathrm{d}x \tag{46}$$

References

Abeles M. (1991), *Corticonics*, Cambridge University Press

Braitenberg V., Schüz A. (1991), *Anatomy of the cortex. Statistics and geometry*, Springer, Berlin

Buchanan J.J., Kelso J.A.S., de Guzman G.C. (1997), The selforganization of trajectory formation: I. Experimental evidence, Biol. Cybern. 76, 257-273

Carson R., Byblow W., Goodman D. (1994), The dynamical substructure of bimanual coordination, in: Swinnen S., Heuer H., Massion J., Casaer P., eds., *Interlimb coordination: Neural, Dynamical and Cognitive Constraints*, pp. 319-337, Academic Press, San Diego

Collins J.J., Stewart I.N. (1993), Coupled nonlinear oscillators and the symmetries of animal gaits, J. Nonlinear Sci. 3, 349-392

Cross M.C., Hohenberg P.C. (1993), Pattern formation outside of equilibrium, Rev. Mod. Phys. 65, 851

Felleman D.J., Van Essen D.C. (1991), Distributed hierarchical processing in the primate cerebral cortex, Cerebral Cortex 1, 1-47

Freeman W.J. (1992), Tutorial on neurobiology: From single neurons to brain chaos, Inter. J. Bif. Chaos 2, 451-482

Friedrich R., Fuchs A., Haken H. (1991), Spatiotemporal EEG patterns, in: Haken H., Koepchen H.P., eds., *Rhythms in Physiological Systems*, Springer, Berlin

Fuchs A., Haken H. (1988), Pattern recognition and associative memory as dynamical processes in a synergetic system I+II, Erratum, Biol. Cybern. 60, 17-22, 107-109, 476

Fuchs A., Kelso J.A.S., Haken H. (1992), Phase Transitions in the Human Brain: Spatial Mode Dynamics, Inter. J. Bif. Chaos 2, 917-939

Haken H., Kelso J.A.S., Bunz H. (1985), A Theoretical Model of Phase transitions in Human Hand Movements, Biol. Cybern. 51, 347 - 356

Haken H. (1983), *Synergetics. An Introduction*, 3rd ed., Springer, Berlin

Haken H. (1987), *Advanced Synergetics*, 2nd ed., Springer, Berlin

Haken H. (1991), *Synergetic Computers and Cognition, A Top-Down Approach to Neural Nets*, Springer, Berlin

Haken H. (1996), *Principles of brain functioning*, Springer, Berlin

Jirsa V.K., Friedrich R., Haken H., Kelso J.A.S. (1994), A theoretical model of phase transitions in the human brain, Biol. Cybern. 71, 27-35

Jirsa V.K., Friedrich R., Haken H. (1995), Reconstruction of the spatio-temporal dynamics of a human magnetoencephalogram, Physica D 89, 100-122

Jirsa V.K., Haken H. (1996), Field theory of electromagnetic brain activity, Phys. Rev. Let. 77, 960

Jirsa V.K., Haken H. (1996), Derivation of a field equation of brain activity, J. Biol. Phys. 22, 101-112

Jirsa V.K., Haken H. (1997), A derivation of a macroscopic field theory of the brain from the quasi-microscopic neural dynamics, Physica D 99, 503-526

Kelso J.A.S. (1981), On the oscillatory basis of movement, Bull. Psychon. Soc. 18, 63

Kelso J.A.S. (1984), Phase transitions and critical behavior in human bimanual coordination, Am. J. Physiol. 15, R1000-R1004

Kelso J.A.S., Scholz J.P., Schöner G. (1986), Nonequilibrium phase transitions in coordinated biological motion: critical fluctuations, Phys. Let. A 118, 279-284

Kelso J.A.S., Buchanan J.J., Wallace S.A. (1991), Order parameters for the neural organization of single, multijoint limb movement patterns, Exp. Brain Res. 85, 432-444

Kelso J.A.S., Bressler S.L., Buchanan S., DeGuzman G.C., Ding M., Fuchs A., Holroyd T. (1992), A Phase Transition in Human Brain and Behavior, Phys. Let. A 169, 134 - 144

Kelso J.A.S., Fuchs A., Holroyd T., Cheyne D., Weinberg H. (1994), Bifurcations In human brain and behavior, Society for Neuroscience , 20, 444

Kelso J.A.S. (1995), Dynamic Patterns. The Self-Organization of Brain and Behavior, The MIT Press, Cambridge, Massachusetts

Kristeva R., Cheyne D., Deecke L. (1991), Neuromagnetic fields accompanying unilateral and bilateral voluntary movements: Topography and analysis of cortical sources, Electroenceph. Clin. Neurophys. 81, 284-298

Miller R. (1987), Representation of brief temporal patterns, Hebbian synapses, and the left-hemisphere dominance for phoneme recognition, Psychobiology 15 , 241-247

Nunez P.L. (1974), The brain wave equation: A model for the EEG, Mathematical Biosciences 21, 279-297

Nunez P.L. (1995), Neocortical dynamics and human EEG rhythms, Oxford University Press

Scholz J.P., Kelso J.A.S., Schöner G. (1987), Nonequilibrium phase transitions in coordinated biological motion: critical slowing down and switching time, Phys. Let. A 123, 390-394

Schöner G., Jiang W.Y., Kelso J.A.S. (1990), A Synergetic Theory of Quadrupedal Gaits and Gait Transitions, J. theor. Biol. 142, 359-391

Tuller B., Kelso J.A.S. (1989), Environmentally-specified patterns of movement coordination in normal and split-brain subjects, Exp. Brain Res. 75, 306-316

Wallenstein G.V., Kelso J.A.S., Bressler S.L. (1995), Phase transitions in spatiotemporal patterns of brain activity and behavior, Physica D 84, 626-634

Wiesendanger M., Wicki U., Rouiller E. (1994), Are there unifying structures in the brain responsible for interlimb coordination?, in: Swinnen S., Heuer H., Massion J., Casaer P., eds., *Interlimb coordination: Neural, Dynamical and Cognitive Constraints*, pp. 179-207, Academic Press, San Diego

Williamson S.J., Kaufman L. (1987), Analysis of neuromagnetic signals, in: Gevins A.S., Remond A., eds., *Methods of analysis of brain electrical and magnetic signals. EEG Handbook*, Elsevier Science

Wilson H.R., Cowan J.D. (1972), Excitatory and inhibitory interactions in localized populations of model neurons, Biophysical Journal 12, pp. 1-24

Wilson H.R., Cowan J.D. (1973), A mathematical theory of the functional dynamics of cortical and thalamic nervous tissue, Kybernetik 13, 55-80